Petroleum Science 20 (2023) 3301–3310

Contents lists available at ScienceDirect

Petroleum Science

journal homepage: www.keaipublishing.com/en/journals/petroleum-science

Original Paper

Tight sandstone gas accumulation mechanisms and sweet spot prediction, Triassic Xujiahe Formation, Sichuan Basin, China

Lin Jiang, Wen Zhao*, Dong-Mei Bo**, Feng Hong, Yan-Jie Gong, Jia-Qing Hao

Research Institute of Petroleum Exploration and Development, PetroChina, Beijing, 100083, China

ARTICLE INFO

Article history:
Received 26 September 2022
Received in revised form
26 January 2023
Accepted 10 July 2023
Available online 10 July 2023

Edited by Jie Hao and Teng Zhu

Keywords:
Tight sandstone gas
Hydrocarbon migration and accumulation
Physical experiment
Numerical simulation

ABSTRACT

The prediction of continental tight sandstone gas sweet spots is an obstacle during tight sandstone gas exploration. In this work, the classic physical fluid charging experimental equipment is improved, the combination of the gas migration and accumulation process with the pore network numerical simulation method is investigated, and application of the permeability/porosity ratio is proposed to predict the gas saturation and sweet spots of continental formations. The results show that (1) as the charging pressure increases, the permeability of the reservoir increases because more narrow pore throats are displaced in the percolation process; and (2) based on pore network numerical simulation and theoretical analysis, the natural gas migration and accumulation mechanisms are revealed. The gas saturation of tight sandstone rock is controlled by the gas charging pressure and dynamic percolation characteristics. (3) The ratio of permeability/porosity and fluid charging pressure is proposed to predict the gas saturation of the formation. The ratio is verified in a pilot and proven to be applicable and practical. This work highlights the tight sandstone gas migration and accumulation mechanisms and narrows the gap among microscale physical experiments, numerical simulation research, and field applications.

© 2023 The Authors. Publishing services by Elsevier B.V. on behalf of KeAi Communications Co. Ltd. This is an open access article under the CC BY-NC-ND license (http://creativecommons.org/licenses/by-nc-nd/4.0/).

1. Introduction

Natural gas is an important link for realizing the transition from traditional fossil energy to clean energy (Zhao et al., 2020; Jia et al., 2021a,b,c). From 2005 to 2021, carbon dioxide emissions of the U.S. power sector fell 32 percent, and nearly two-thirds of that were derived from replacing coal with natural gas (Dudley, 2018; Zhao and Du, 2019). Natural gas is essential in achieving the “dual carbon goals” and “beautiful China” in China. However, natural gas accounts for a relatively low proportion of China’s primary energy consumption structure. In 2020, natural gas consumption in China was 3.073×10^{11} m^3, accounting for only 7.8% of primary energy consumption (Li et al., 2017; Jiang et al., 2021a,b). Tight sandstone gas is widely distributed in the world's major petrol-bearing basins. The development of tight sandstone gas has skyrocketed in China in recent years. However, the exploration and development of tight sandstone gas in China are restricted by an insufficient understanding of the accumulation mechanism and difficulty in predicting sweet spots. Investigating the tight sandstone gas accumulation mechanisms and proposing a practical sweet spot prediction method are vital.

Tight sandstone gas shows abnormal characteristics that are different from those of conventional reservoirs. Theories of tight sandstone gas date to 1976, when geologists discovered the Elmworth Gas Field in a deep depression in the western Alberta Basin. Canadian geologist Master (1979) proposed the theory of deep basin gas. However, during tight sandstone gas exploration, petroleum geology theories developed for conventional formations cannot be directly transferred to tight sandstone gas. The lack of petroleum geology theory for tight sandstone gas has become an obstacle during the exploration and development of tight sandstone gas (Zhao et al., 2021; Zhu et al., 2022). Unlike the tight sandstone gas reservoirs in south Texas (North America), South America, or the Middle East, most of the tight sandstone gas reservoirs in China are deposited in continental facies or transitional facies (Jia et al., 2021a,b,c). The migration and swing of rivers are frequent, resulting in a complex sand body superimposition relationship and gas/water distributions (Pang et al., 2021), which makes the prediction of sweet spots of tight reservoirs more

* Corresponding author.
** Corresponding author.
E-mail addresses: zhaow22@petrochina.com.cn (W. Zhao), bdmei@petrochina.com.cn (D.-M. Bo).

https://doi.org/10.1016/j.petsci.2023.07.008
1995-8226/© 2023 The Authors. Publishing services by Elsevier B.V. on behalf of KeAi Communications Co. Ltd. This is an open access article under the CC BY-NC-ND license (http://creativecommons.org/licenses/by-nc-nd/4.0/).

complex. Some methods may be helpful and practical in North America. However, they are not suitable for tight sandstone gas in China. There is a need to develop a series of theories and methods for tight continental gas during the exploration and development process, especially for sweet spot prediction in China.

Previous researchers have conducted much work on tight sandstone gas migration and the accumulation process. From early studies on deep basin gas (Sneider et al., 1978) to recent research on tight sandstone gas (Jiang et al., 2021a,b; Jia et al., 2022), researchers have paid much attention to the distribution of source rocks (Al-Mahmoud et al., 2010), the hydrocarbon-generating intensity of source rocks (H. Jiang et al., 2015), reservoir quality (Busch et al., 2019), and pore structure (Qiao et al., 2020; Jia et al., 2021a,b,c). These studies are meaningful and guide the exploration and development of tight sandstone gas in the early stage. However, under the pressure of poor oil prices, highly qualified exploration and development places higher requirements on the sweet spot prediction method, which guides people's attention to further research on tight formation. Physical experiments (Z. Jiang et al., 2015) and numerical simulations (Freeman et al., 2013; Jia et al., 2021a,b,c) are employed to reveal the mechanism of the fluid charging and migration process. The effects of charging pressure (Comisky et al., 2007), pore structure (Sakhaee-Pour and Bryant, 2014; Lai and Wang, 2015), and fluid flow dynamics (Rushing et al., 2003; Wood and Sanei, 2016) are discussed. All these works highlight tight sandstone gas migration and the accumulation mechanisms. However, there exists a gap between microscale research and field application. Although researchers have gained much micro recognition of the hydrocarbon migration and accumulation process, these theories are still confined to the lab. Petroleum geologists still use traditional and rough methods to practically predict the sweet spots of tight formations (Huo et al., 2022). Physical experiments are only suitable for real cores, and numerical simulations primarily simulate microphenomena (Liu et al., 2020; Zhao et al., 2021).

Nevertheless, there are still obstacles between physical experiments and numerical simulation methods. This work is aimed at narrowing the gap between physical experiments and numerical simulation methods and revealing the tight sandstone gas accumulation mechanisms. Based on the physical experiment and numerical simulation results, a novel factor is proposed to predict the sweet spot of a tight formation, which will be more applicable and practical.

The paper structure is organized as follows: The physical experiment and numerical simulation methods are introduced in Section 3. The results are given in Section 4. In Section 5, the dynamic mechanisms of tight sandstone gas migration and accumulation are revealed. The sweet spot prediction method is verified based on the field application in Section 6. Conclusions are summarized in Section 7.

2. Geological background

In this work, the Hechuan area, which is located in the Sichuan Basin, is chosen as the pilot area, and all real rock cores are obtained from this area (Fig. 1). The Hechuan gas field has experienced a sedimentary and tectonic evolution history similar to that of the main body of the Sichuan Basin. Marine strata dominated by carbonate rocks below the Middle Triassic and continental strata from the Upper Triassic to Neogene were deposited. The Hechuan gas field has also experienced Caledonian, Hercynian, Indonesian, Yanshan, and Himalayan tectonic movements. The Indosinian, Yanshan and Himalayan movements have an essential influence on the formation of the Hechuan gas field (Guo et al., 2019).

The outcrop layer of the Hechuan gas field is the dark purple mudstone of the Upper Jurassic Suining Formation. The Upper Jurassic Suining Formation, Middle Shaximiao Formation, Lower Liangshan Formation, Ziliujing Formation, Upper Triassic Xujiahe Formation, and Middle Triassic Leikoupo Formation were successively debunked from top to bottom. The stratigraphic sequence was typical. In the Hechuan area, the source rocks are mainly distributed in Member 1, Member 3, and Member 5 of the Xujiahe Formation. Moreover, hydrocarbons mainly accumulate in Member 2 and Member 4. From the spatial distribution of source rock and reservoir formation, the hydrocarbon migrates from the bottom formation (Member 3 and Member 5 of Xujiahe Formation) and accumulates in the upper formation (Member 2 and Member 4 of Xujiahe Formation).

The second member of the Xujiahe Formation in this area mainly belongs to delta front subfacies deposition, and the delta front underwater distributary channel and mouth bar are the central reservoir sand bodies. The microfacies of the underwater distributary channel and the mouth bar of the delta front in the Hechuan area are closely symbiotic in space and constitute the skeleton sand body of the delta front (Fig. 1).

3. Methodology

3.1. Physical experiment facility development

As a classic research method, fluid charging physical experiments reveal fluid dynamics based on artificial or natural rock cores. However, for tight rock, a physical experiment can hardly meet the accuracy requirement of measurement. In this work, a variable volume fluid charging facility is developed to improve the range of equipment. In this section, the relationships between pressure and permeability and gas saturation of the tight rock core with the improved facility is investigated.

The unsteady gas measurement method is usually applied to measure the permeability of low permeability rock to ultralow permeability rock, and the measurement range is usually less than 1 mD. However, the variation range of tight sandstone reservoirs exceeds this limit, and the permeability in some reservoirs is not only 1 mD but also greater than 1 mD. Conventional measurements are required for these samples with permeabilities greater than 1 mD, which can produce systematic errors. It is difficult for classic physical experimental equipment to obtain accurate data. In this work, variable volume measuring tanks are added as a bridge between the injecting tank and the core holder, which will increase the accuracy of the fluid charging facility. The primary fluid charging physical experiment diagram is shown in Fig. 2, and the experimental steps are listed as follows:

(1) The tight rock core is put into the core holder, and the confining pressure pump is opened to simulate the pressure condition underground;
(2) The gas valve is opened, and natural gas is injected into the variable volume measuring tank, which is connected to the injection pump;
(3) The gas valve is closed, the injection pump is opened, and the water is injected into the tank;

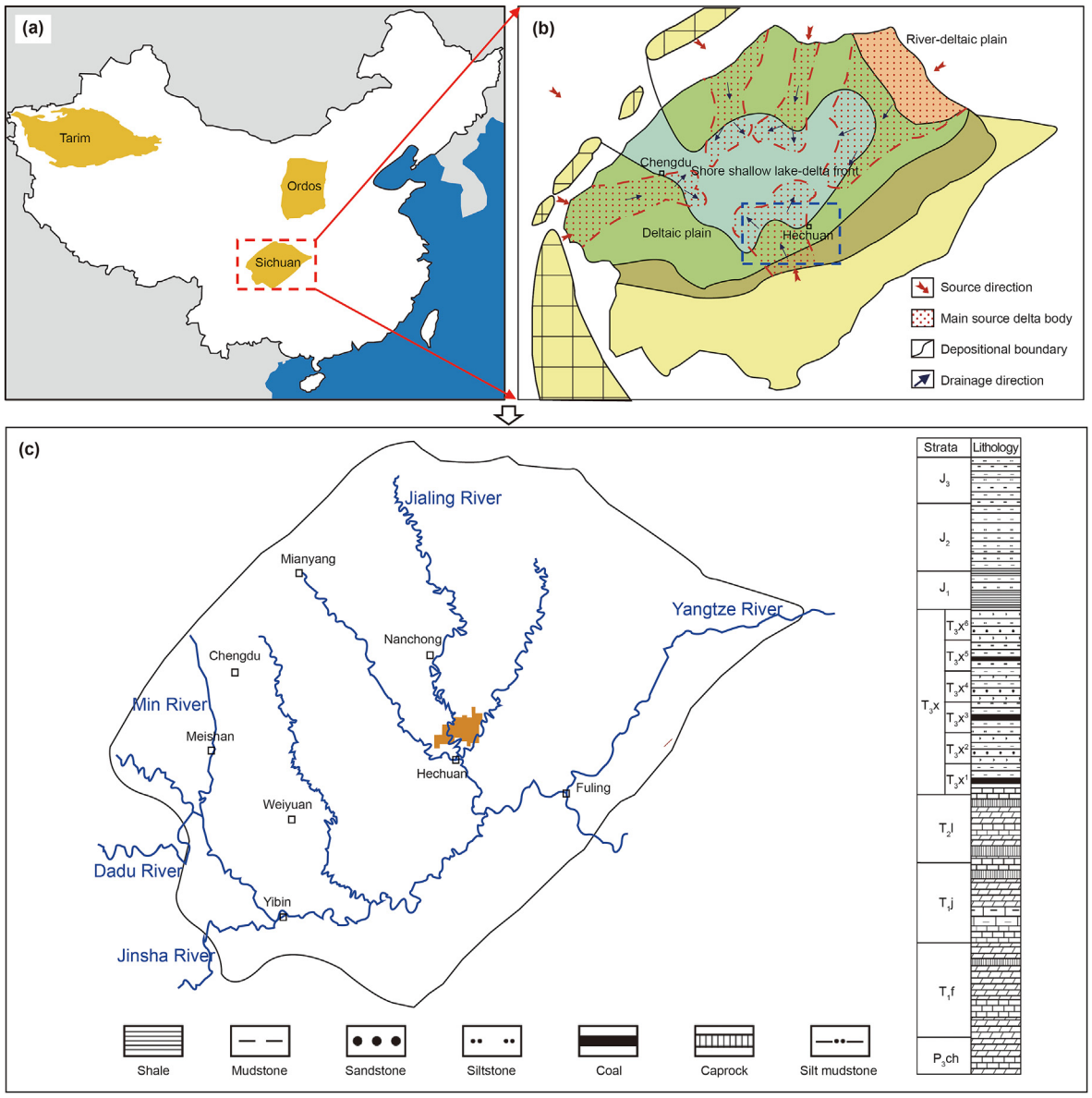

Fig. 1. (a) Map of the main sedimentary basins of China. (b) Sedimentary facies of the second member of the Xujiahe Formation, Sichuan Basin. The red arrows show the source directions. The blue arrows show the drainage directions. The mesh areas show the main source delta bodies. (c) Location of Hechuan Area in Sichuan Basin.

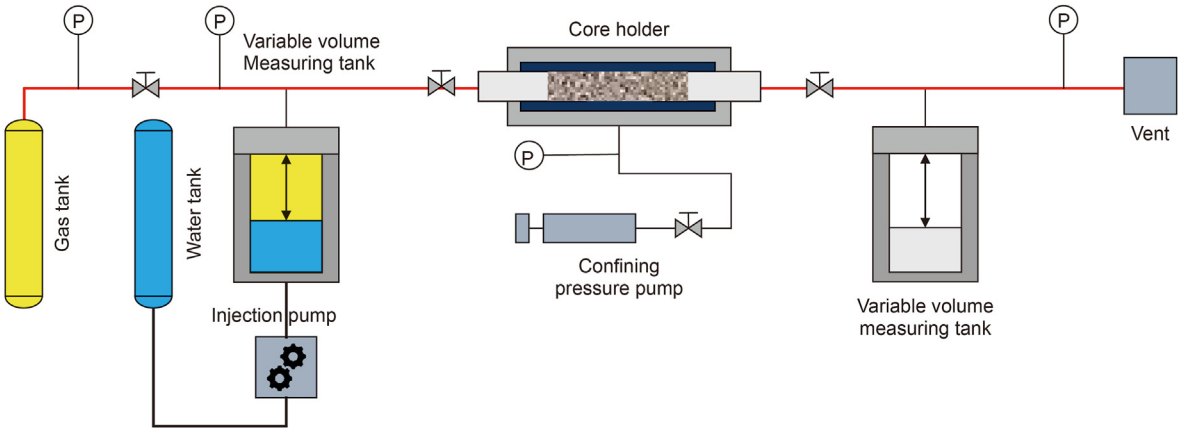

Fig. 2. Variable volume fluid charging facility. The underground conditions are simulated by a confining pressure pump and thermostat. Two variable volume measuring tanks are utilized to meet the accuracy of the physical experiment for tight rock. Furthermore, gas is indirectly injected by the water injection pump.

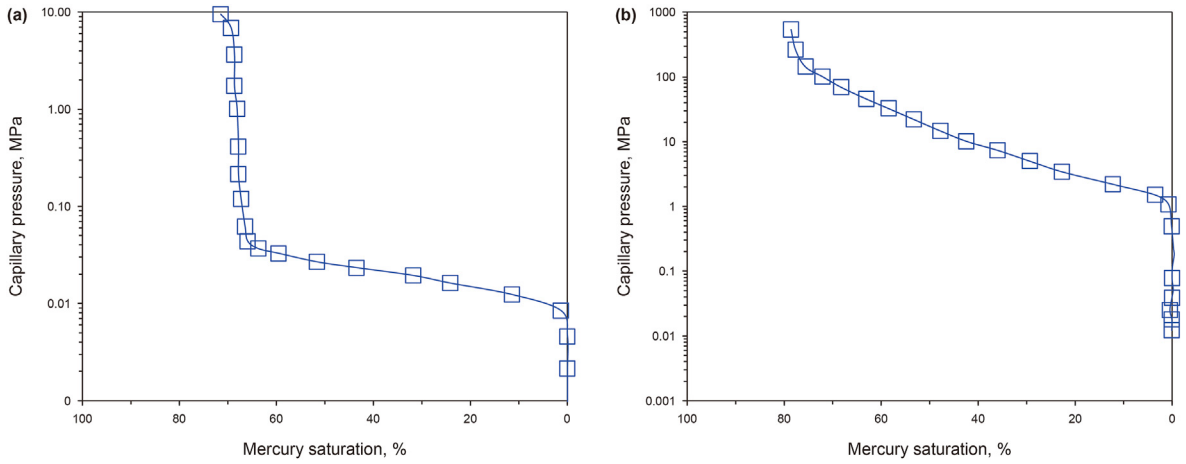

Fig. 3. Capillary curves of conventional and tight sandstone rock cores. (a) the capillary curve of a conventional rock core. (b) the capillary curve of a tight rock core. There are apparent differences between the two curves in morphology. For conventional rock cores, capillary pressure slowly increases at low mercury saturation but rapidly rises in the high mercury saturation region. Nevertheless, for tight sandstone rock cores, the capillary pressure always rapidly increases in the process of increasing mercury saturation.

(4) The injected water will displace the gas in the variable volume measuring tank;
(5) The flux and pressure data will be measured by the number of sensors in the connections of pipes utilized in this physical experiment.

3.2. Pore network numerical simulation method

Two methods can generate the pore network (PNM): (1) a regular model generated by the algorithm (He et al., 2021a,b) and (2) an irregular model extracted by the information from the micron CT image (Zhao et al., 2023). Both methods have their own merits. This work is restricted to the dynamic mechanisms of tight sandstone gas charging. To obtain more interconnected pores, a regular model based on the capillary curve is adopted.

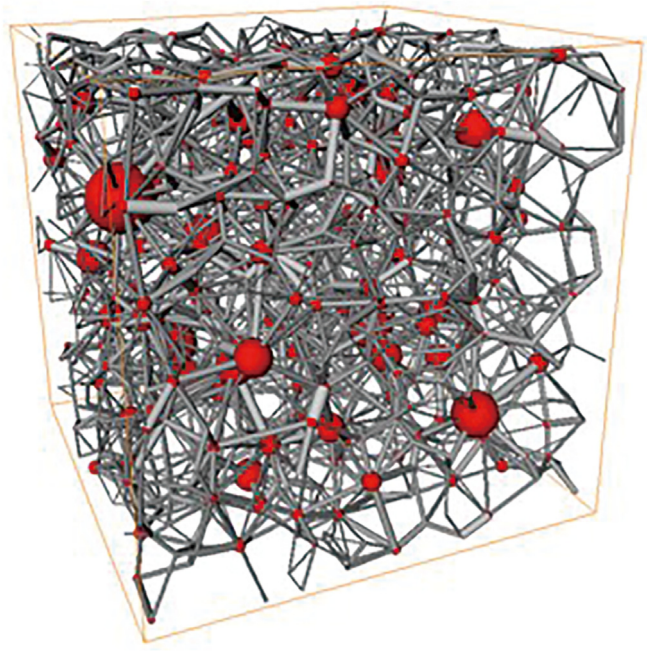

Fig. 4. Pore network of tight rock. The red balls show the model's pore, and the size variation shows the volume variation. The gray areas show the distribution of throats, and the changing radius of the cylinder shows the geometrical variation in the throats.

Capillary curves typically describe the pore structure with the mercury injection method. Fig. 3 shows two typical capillary curves. Fig. 3a shows the capillary curve of a conventional rock core, and Fig. 3b shows the capillary curve of a tight rock core. There are apparent differences between the two curves in morphology. For conventional rock cores, capillary pressure slowly increases at low mercury saturation but rapidly rises in the high mercury saturation region. Nevertheless, for tight sandstone rock cores, the capillary pressure always rapidly increases with increasing mercury saturation.

According to a physical capillary curve (Fig. 3b) of a tight rock core from the Triassic Xujiahe Formation, Sichuan Basin, the pore network model is generated (Fig. 4). The variation in size shows the variation in volume. The gray areas show the distribution of throats, and the changing radius of the cylinder shows the geometrical variation in the throats.

The PNM is generated according to the real core from the Xujiahe Formation (2240.0 m). The porosity of the real sample is 10.31%, the permeability is 0.12 mD, the porosity of the generated PNM is 10.12%, and the permeability is 0.12 mD. The similarity among them is high, which indicates that the generated pore network model is consistent with the actual situation.

4. Results

4.1. Gas saturation under different charging pressures

Section 3.1 introduces the physical experiment facility and process. In this work, the fluid charging pressures are changed, and the tight rock core gas saturation under different injection pressures is analyzed. Fig. 5 shows the variation in the inlet pressure during the injection process.

Four stages are observed when the gas is steadily charged in each experiment. Stage A: in this stage, the pressure accumulates in the inlet. During this stage, according to the Young-Laplace equation (Eq. (1)), the gas cannot overcome the resistance of capillary pressure. Stage B: in this stage, the gas is injected into the tight rock core, and the water in the core is rapidly displaced. Stage C: in this stage, the gas is steadily injected into the tight rock core. Stage D: in this stage, the gas phase breaks through the outlet section.

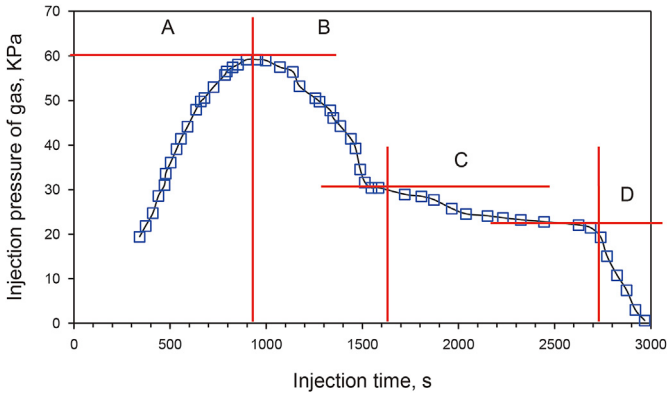

Fig. 5. Pressure data of a typical physical experiment condition. The Y-axis shows the gas injection pressure, and the X-axis shows the injection time. The gas is injected indirectly by the injected water, and the flux of injection water is 0.1 mL/min. The blue plots show the injection pressure of the gas during the injection process.

$$p_c = \frac{2\sigma \cos\theta}{r} \tag{1}$$

where p_c is the capillary pressure in MPa and σ represents the interface tension between the insoluble fluids in mN/m. In this work, the interface tension between gas and water is 72.5 mN/m, and θ is the contact angle of the tight rock core; here, it is 42°, and r is the pore radius.

In the natural geological background, the gas charging process is controlled by the source rock distribution or by the natural gas charging pressure. The injection pressure of gas is changed to reconstruct the actual geological condition and analyze the relationships between the flow dynamics in tight rock and its physical properties.

The permeability of the tight rock is calculated by Darcy's Law (Zhang et al., 2020):

$$K = \frac{qA\partial P}{\mu \partial l} \tag{2}$$

where K is the permeability of the tight rock core, mD; q is the flux of the fluid phase, mL/s; μ is the viscosity of fluids, mPa·s; and $\partial P/\partial l$ is the pressure difference between the inlet of the core and the outlet of the core. In this work, according to Darcy's Law, the permeability varies with the fluid charging pressure.

As shown in Fig. 6, both the gas saturation and permeability of the tight rock core increase with increasing fluid charging pressure. However, their increasing modes show some differences. In Fig. 6, the gas saturation gradually increases with the charging pressure, rapidly increases in the range of 0–4 MPa, and slowly increases after 6 MPa. The permeability slowly initially increases from 0–2 MPa, rapidly increases in the range of 3–6 MPa, rapidly increases; after 7 MPa, and then slowly increases with increasing charging pressure.

As the charging pressure increases, the permeability of the reservoir increases because narrower pore throats are involved in the seepage process. Accordingly, with increasing charging pressure, the gas saturation shows a gradual increase. The experimental results show a positive correlation between gas saturation and the permeability/porosity ratio. Further analysis is revealed in Section 4 regarding the theory and numerical simulation method.

Fig. 7 shows the physical experiment of an artificial core. The artificial core shows lower heterogeneity and better regularity than the real rock core. With increasing charging pressure, the permeability of the artificial core also gradually increases.

4.2. Numerical simulation of pore network charging

In the process of natural gas charging in tight sandstone rock, natural gas must overcome the capillary pressure of the pores and throats. Under the initial conditions, the pore network model is saturated with water. Then, the gas is charged into the pore network model from the bottom to simulate the charging process. Fig. 8 shows snapshots of the gas charging dynamic process and the fluid distribution of gas and water under different charging pressures. The results are visualized in this numerical simulation. Red represents the pores and throats that have been filled with gas. Blue indicates that the water or throats have not filled with gas. Spheres represent pores, whose diameters represent pore sizes. The cylinder represents the throat, and its length and diameter indicate the length and width of the throat.

During the early stage of natural gas charging, when the charging pressure is only 10 MPa, the natural gas can only overcome the larger pores/throats whose capillary pressure is less than 10 MPa. First, gas is charged into the pore network by connecting larger pores, and the charging front appears. Although some pores

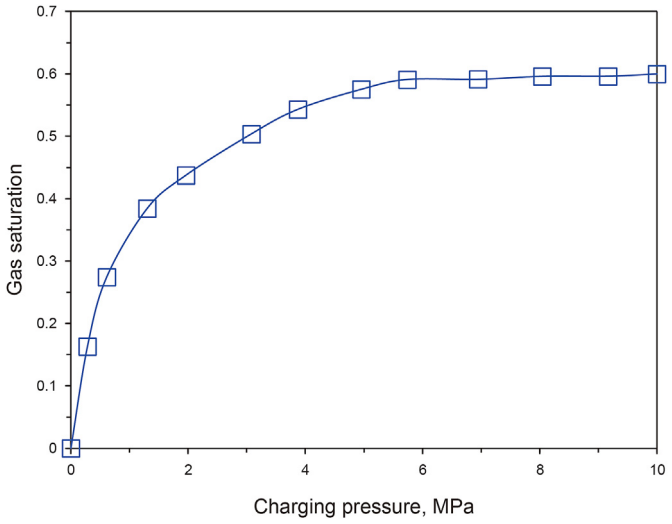

Fig. 6. Relationships among gas saturation, permeability, and fluid charging pressure. The blue plots represent physical experiment data. This figure shows the relationship between gas saturation and charging pressure; the gas saturation increases with increasing pressure.

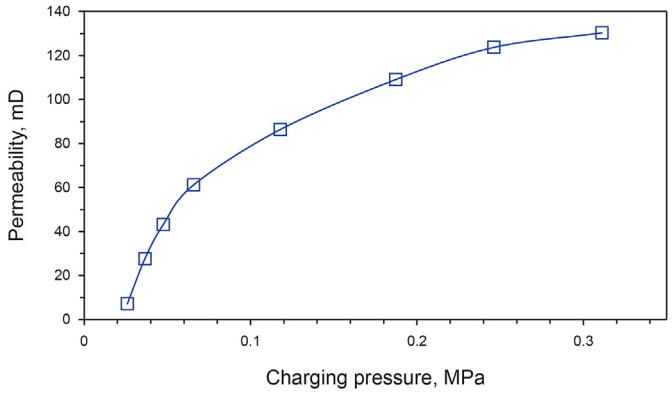

Fig. 7. Relationship between the permeability of the artificial core and the charging pressure. Compared to the real rock core, the artificial core shows lower heterogeneity and better regularity. With increasing charging pressure, the permeability of the artificial core also increases.

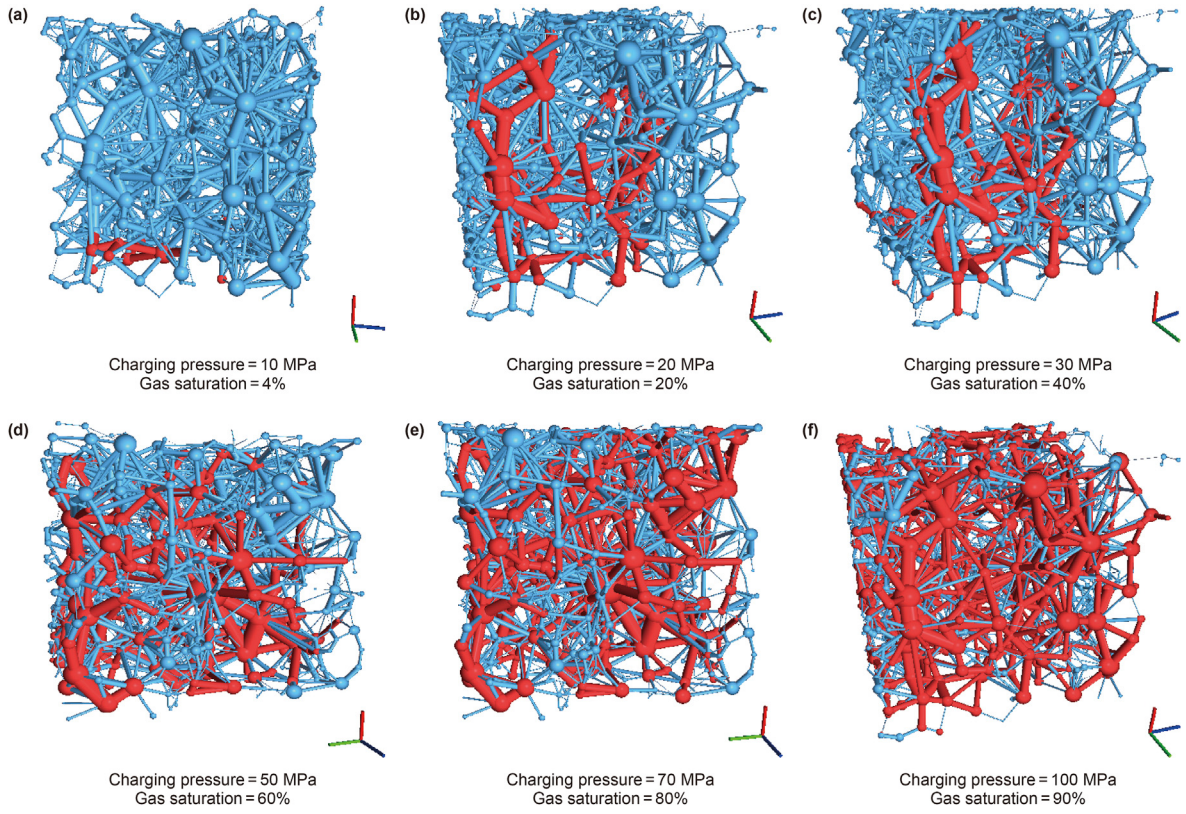

Fig. 8. Snapshots of the gas charging dynamic process. Red indicates natural gas, and blue indicates water. (a)–(f) Fluid distribution under different charging pressures.

at the bottom are filled with gas, due to the smaller throat size connected to them and high capillary resistance, the gas cannot be immediately pushed forward after filling (Fig. 8a).

5. Discussions

5.1. Dynamic mechanisms of tight sandstone gas migration and accumulation

The pore network numerical simulation method is referred to as a guaranteed method to study dynamic phenomena in porous media (He et al., 2021a, b). In this section, the tight rock core network is reconstructed, and the flow dynamics in the pore network are simulated. A novel factor is proposed to describe the flow dynamics and predict the gas saturation of tight rock.

With increasing charging pressure, more gas is charged into the pore network, the gas saturation in the pore network model increases, and the gas-water boundary advances (Fig. 8a and b). The migration mode tends to be finger-like. When the charging pressure reaches 30 MPa, the gas phase communicates the outlet and inlet of this pore network model (Fig. 8c). Charging pressure is not a constant during the hydrocarbon migration and accumulation process; 50 MPa is almost the maximum pressure that can be achieved by charging pressure during the process of hydrocarbon migration and accumulation in the Hechuan area of the Sichuan Basin (Jiang et al., 2016). As shown in Fig. 8d, when the charging pressure increases to 50 MPa, the gas saturation reaches 60%, which is consistent with the natural tight rock formation in the Hechuan area of the Sichuan Basin. At this stage, the larger pores are almost entirely charged. Note that due to the heterogeneity characteristics of the pore network, only some of the macropores are initially filled.

For the water phase, natural gas is gradually charged into the pore network, pore water is gradually displaced, and the number of water-bearing pores decreases (Fig. 8a–d). When gas is charged into the pore network, connected water in the large pores is displaced (Fig. 8a and b). As the charging continued, the medium-size pores were gradually charged (Fig. 8b and c). After filling, water is mainly residual in tiny pores and narrow throats (Fig. 8e and f). Note that a small amount of water is also residual in large pores connected with tiny pores or narrow throats, which cannot be filled by natural gas.

5.2. Relationships between gas saturation and permeability/porosity ratio

From the view of physical experiments and numerical simulation, this work has clearly and directly revealed the natural gas migration and accumulation dynamic process and mechanisms. Further research is also carried out. An exciting phenomenon caught the authors' attention after numerous physical experiment tests with different tight rock cores. Although there is no apparent positive or negative correlation between the permeability and porosity of tight rock (Fig. 9), the ratio of permeability to porosity positively correlates with gas saturation (Fig. 10).

Fig. 10 shows the gas saturation of different permeability/porosity ratios under different gas charging pressures (5 MPa to 50 MPa). Tight rock gas saturation positively correlates with the permeability/porosity ratio. According to the apparent correlation, the analytical equation that describes the relationship between permeability and porosity is obtained by numerical fitting, as shown by the colorful lines. For instance, when the charging pressure is 5 MPa, the core gas saturation increases when the permeability/porosity ratio increases.

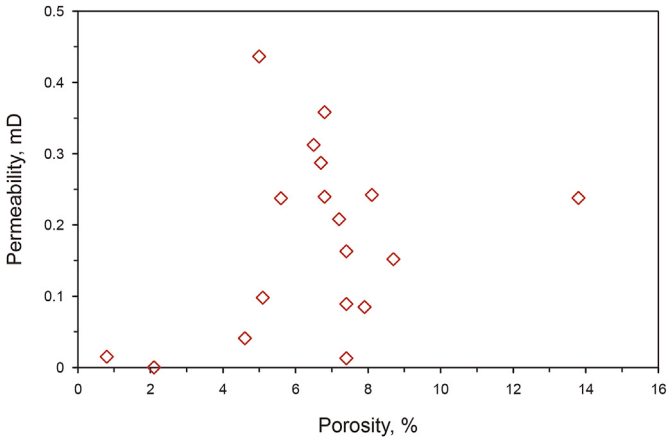

Fig. 9. Relationships between permeability and porosity of tight sandstone rock core in Hechuan area of the Sichuan Basin. The red plots show the data on porosity and permeability. There is no apparent positive or negative correlation relationship between the permeability and porosity of tight rock in the Hechuan area of the Sichuan Basin.

As shown in Fig. 10, different color spots indicate the experimental data for different charging pressures. The gas saturation is consistent with the ratio of permeability/porosity under different charging pressures. The ratio of permeability/porosity indicates both the heterogeneity characteristics of the reservoir and the influence of the pore structure on natural gas charging. In essence, the ratio expresses the difference in seepage channels in the rock during natural gas filling. The difference between the percolation channels and the reservoir space results in the difference in gas saturation.

6. Field application

According to previous physical experiments and numerical simulation analyses, the gas saturation of tight sandstone rock is controlled by the gas charging pressure and dynamic percolation characteristics. Combining the ratio of permeability to porosity with the fluid charging pressure is proposed to predict the formation saturation. This method is novel and applicable and has already been validated as useful in the field. In this section, two field application cases are shown: the first case is the gas saturation prediction of the developed fields for enhancing gas recovery, and the second case is the sweet spot prediction of a developing field for tight sandstone gas exploration and development.

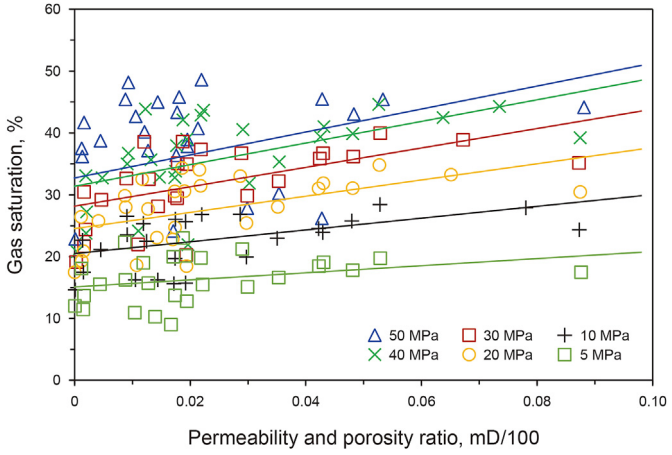

Fig. 10. Relationship between gas saturation and the permeability/porosity ratio. The colorful plots show the physical experiment data. The analytical equation for this relationship is obtained by numerical fitting, as shown by the lines, according to the apparent correlation.

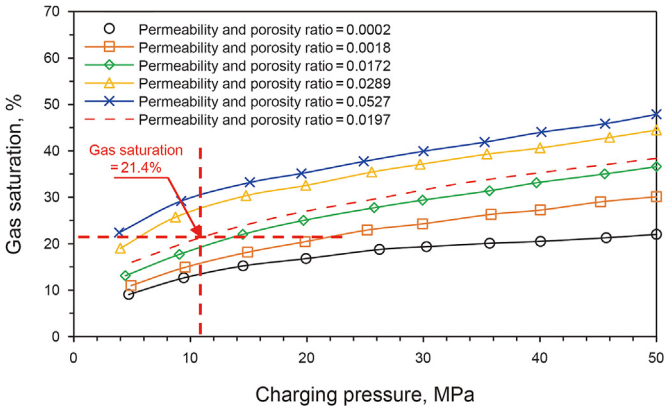

Fig. 11. Gas saturation prediction chart. The Y-axis shows the predicted gas saturation of tight rock; the X-axis indicates the fluid charging pressure during gas migration and accumulation. The lines show the relationships between gas saturation and fluid charging pressure with different permeability/porosity ratios.

Table 1
Well-logging data of the HC-5 well.

Measured depth, m	2261.3
Kelly bushing, m	357.21
Formation pressure, MPa	30.07
Charging pressure, MPa	11.03
Porosity	7.41%
Permeability, mD	0.1457
Porosity/Permeability ratio	0.0197
Gas saturation	21.93%

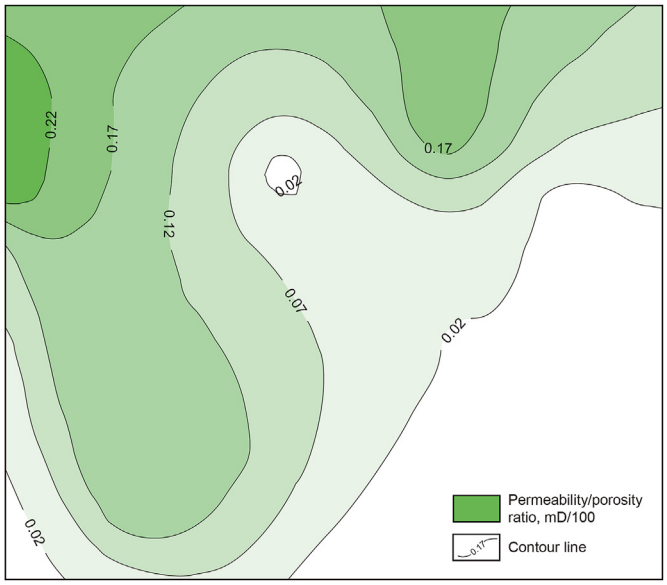

Fig. 12. Distribution of the ratio of permeability to porosity. Dark green indicates the area with a larger permeability/porosity ratio; light green indicates the area with a smaller permeability/porosity ratio.

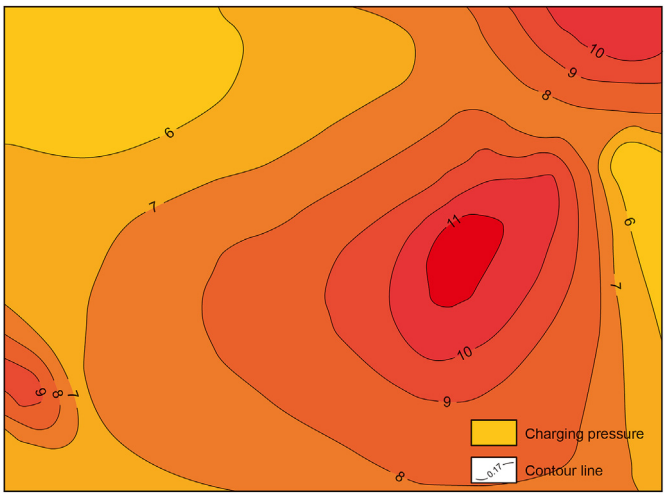

Fig. 13. Distribution of charging pressure.

6.1. Gas saturation prediction

According to the proposed gas saturation prediction method, a prediction chart is established in this section. As shown in Fig. 11, the lines show the relationships between gas saturation and fluid charging pressure with different permeability/porosity ratios. The usage of the chart is described as follows:

(1) The regional physical properties are obtained by core test experiments;
(2) According to the ratio of permeability to porosity, the corresponding curve is searched;
(3) Gas saturation is predicted based on charging pressure; if it is difficult to obtain the fluid charging pressure during the gas migration and accumulation process, the tubing pressure can be applied in this step.

Table 1 shows the well logging data of Well HC-5. The charging pressure of Well HC-5 is 11.03 MPa, and the porosity/permeability ratio is 0.0197. Referring to Fig. 11, when the porosity/permeability ratio is 0.0197, the predicted gas saturation of Well HC-5 is 21.4%, and the logging interpretation of gas saturation is 21.93%. The predicted value shows agreement with the actual value. The proposed gas saturation is valuable and valid. However, this accurate gas saturation requires much experimental data to establish the gas saturation chart. At the beginning of tight sandstone gas exploration and development, this method was limited but instructive.

6.2. Sweet spot prediction

As shown in Section 5.1, if the gas reservoir has been developed for a while the gas saturation prediction chart can be established to predict the gas saturation of the new well to enhance the gas recovery. However, if the area needs to be better explored, then petroleum geologists can combine the charging pressure and porosity/permeability ratio to predict the sweet spots of tight formations.

This section introduces an actual field application case to validate the authors' sweet spot prediction method. Fig. 12 shows the distribution of the ratio of permeability and porosity; in this area, the ratio of permeability and porosity is more extensive in the northwest region. Fig. 13 shows the distribution of the hydrocarbon charging pressure. The gas charging pressure is higher in the central region. The sweet spots are predicted with the distribution of the permeability/porosity ratio and that of the hydrocarbon charging pressure. As shown in Fig. 14, the green areas are predicted sweet spot regions. After PetroChina Company's years of exploration and development, petroleum geologists and engineers have drilled many wells. Some wells have sound production with commercial value. The locations of these wells are consistent with

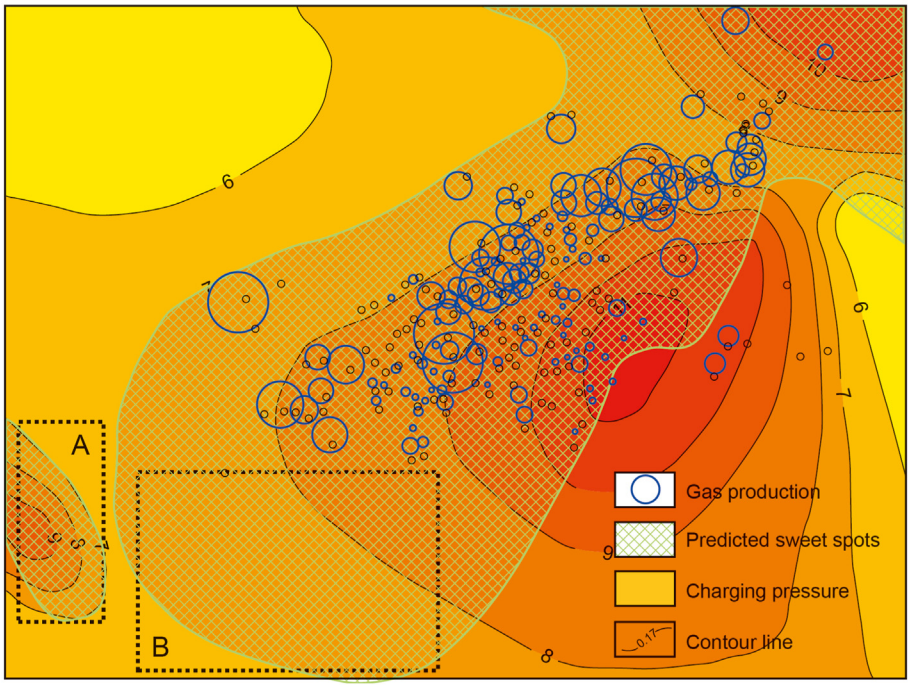

Fig. 14. Distribution of predicted sweet spots and production wells. The green mesh area represents the predicted sweet spots. The blue circle indicates the production of wells; a larger radius indicates more significant gas production.

the authors' prediction regions (Fig. 14). As shown in Fig. 14, the blue circle indicates the production of wells; a larger radius indicates more significant gas production. The mesh areas are predicted sweet spot regions. Almost all high-production wells are in the predicted sweet spot region. However, Areas A and B of the predicted sweet spots still need to be developed, and new wells can be placed in these zones to further enhance the recovery of the reservoir.

Although the predictions are accurate, the sweet spots will have to be adjusted in the gas field exploration and development process. If enough reservoir data is obtained, the petroleum geologist can establish a gas saturation prediction chart to predict the accurate gas saturation of the new well.

7. Conclusions

(1) In this work, a physical simulation technology for tight sandstone gas accumulation is developed, and physical simulation experiments are carried out for tight sandstone gas accumulation based on natural tight sandstone cores. The complex relationship between the gas charging pressure difference and gas saturation is revealed. As the charging pressure increases, the permeability of the reservoir increases because narrower pore throats are involved in the percolation process. Accordingly, with increasing charging pressure, the tight sandstone reservoir gas saturation shows a gradual increase.

(2) The natural gas migration and accumulation mechanisms are clarified based on the PNM numerical simulation and theoretical analysis. The gas saturation of tight sandstone rock is controlled by the gas charging pressure and dynamic percolation characteristics. Combining the ratio of permeability to porosity with fluid charging pressure is proposed to predict the formation saturation.

(3) Combined with the characteristics of charging pressure, the gas saturation chart of a tight sandstone reservoir is established, and the favorable area of tight sandstone gas is predicted. Combined with actual production data, the gas-bearing prediction method proposed in this paper is solid and applicable during hydrocarbon exploration and development.

Declaration of competing interest

No conflict of interest exits in the submission of this manuscript.

Acknowledgments

This work is supported by CNPC Scientific Research and Technology Development Project "Whole petroleum system theory and unconventional hydrocarbon accumulation mechanism" (2021DJ0101).

References

Al-Mahmoud, M.J., Al-Ghamdi, I., 2010. An overview of tight sandstone gas reservoirs in Saudi Arabia. In: Second EAGE Middle East Tight Sandstone Gas Reservoirs Workshop. EAGE, p. 244. https://doi.org/10.3997/2214-4609.20145641.

Busch, B., Becker, I., Koehrer, B., Adelmann, D., Hilgers, C., 2019. Porosity evolution of two Upper Carboniferous tight-gas-fluvial sandstone reservoirs: impact of fractures and total cement volumes on reservoir quality. Mar. Petrol. Geol. 100, 376–390. https://doi.org/10.1016/j.marpetgeo.2018.10.051.

Comisky, J.T., Newsham, K., Rushing, J.A., Blasingame, T.A., 2007. November. A comparative study of capillary-pressure-based empirical models for estimating absolute permeability in tight sandstone gas sands. SPE Annu. Tech. Conf. Exhib. https://doi.org/10.2118/110050-MS.

Dudley, B., 2018. BP Statistical Review of World Energy. BP statistical review, London, UK, 00116. Available via. https://www.bp.com/en/global/corporate/energy-economics/statistical-review-of-world-energy/electricity.html. (Accessed 6 August 2018).

Freeman, C.M., Moridis, G., Ilk, D., Blasingame, T.A., 2013. A numerical study of performance for tight sandstone gas and shale gas reservoir systems. J. Pet. Sci. Eng. 108, 22–39. https://doi.org/10.1016/j.petrol.2013.05.007.

Gou, Q., Xu, S., 2019. Quantitative evaluation of free gas and adsorbed gas content of Wufeng-Longmaxi shales in the Jiaoshiba area, Sichuan Basin, China. Adv. Geo-Energy Res. 3 (3), 258–267. https://doi.org/10.26804/ager.2019.03.04.

He, M., Zhou, Y., Chen, B., Zhang, T., Wu, K., Feng, D., Li, X., 2021a. Effect of pore structure on slippage effect in unsaturated tight formation using pore network model. Energy Fuel. 35 (7), 5789–5800. https://doi.org/10.1021/acs.energyfuels.0c04044.

He, M., Zhou, Y., Wu, K., Hu, Y., Feng, D., Zhang, T., Li, X., 2021b. Pore network modeling of thin water film and its influence on relative permeability curves in tight formations. Fuel 289, 119828. https://doi.org/10.1016/j.fuel.2020.119828.

Huo, F., Chen, Y., Ren, W., Dong, H., Yu, T., Zhang, J., 2022. Prediction of reservoir key parameters in "sweet spot" on the basis of particle swarm optimization to TCN-LSTM network. J. Pet. Sci. Eng. 110544. https://doi.org/10.1016/j.petrol.2022.110544.

Jia, C., Huang, Z., Sepehrnoori, K., Yao, J., 2021a. Modification of two-scale continuum model and numerical studies for carbonate matrix acidizing. J. Pet. Sci. Eng. 197, 107972. https://doi.org/10.1016/j.petrol.2020.107972.

Jia, C., Sepehrnoori, K., Huang, Z., Zhang, H., Yao, J., 2021b. Numerical studies and analysis on reactive flow in carbonate matrix acidizing. J. Pet. Sci. Eng. 201, 108487. https://doi.org/10.1016/j.petrol.2021.108487.

Jia, C., Sepehrnoori, K., Huang, Z., Yao, J., 2021c. Modeling and analysis of carbonate matrix acidizing using a new two-scale continuum model. SPE J. 26 (5), 2570–2599. https://doi.org/10.2118/205012-PA.

Jia, C., Sepehrnoori, K., Zhang, H., Yang, Y., Yao, J., 2022. Numerical investigation of fluid phase momentum transfer in carbonate acidizing. Petrol. Sci. 19 (2), 639–650. https://doi.org/10.1016/j.petsci.2021.11.016.

Jiang, H., Pang, X., Shi, H., Yu, Q., Cao, Z., Yu, R., Jiang, F., 2015. Source rock characteristics and hydrocarbon expulsion potential of the Middle Eocene Wenchang formation in the Huizhou depression, Pearl River Mouth basin, south China sea. Mar. Petrol. Geol. 67, 635–652. https://doi.org/10.1016/j.marpetgeo.2015.06.010.

Jiang, Z., Li, Z., Li, F., Pang, X., Yang, W., Liu, L., Jiang, F.J., 2015. Tight sandstone gas accumulation mechanism and development models. Petrol. Sci. 12 (4), 587–605. https://doi.org/10.1007/s12182-015-0061-6.

Jiang, F., Chen, D., Wang, Z., Xu, Z., Chen, J., Liu, L., Liu, Y., 2016. Pore characteristic analysis of a lacustrine shale: a case study in the Ordos Basin, NW China. Mar. Petrol. Geol. 73, 554–571. https://doi.org/10.1016/j.marpetgeo.2016.03.026.

Jiang, L., Zhao, W., Fan, Y., Hong, F., Gong, Y., Hao, J., 2021a. Effects of micro-fracture and micro-coal line on tight sandstone gas accumulation, Triassic Xujiahe Formation, Sichuan Basin, China. Energy Rep. 7, 7913–7924. https://doi.org/10.1016/j.egyr.2021.08.185.

Jiang, L., Zhao, W., Huang, J., Fan, Y., Hao, J., 2021b. Effects of interactions in natural gas/water/rock system on hydrocarbon migration and accumulation. Sci. Rep. 11 (1), 1–13. https://doi.org/10.1038/s41598-021-01653-0.

Lai, J., Wang, G., 2015. Fractal analysis of tight sandstone gas sandstones using high-pressure mercury intrusion techniques. J. Nat. Gas Sci. Eng. 24, 185–196. https://doi.org/10.1016/j.jngse.2015.03.027.

Li, X., Liang, J., Xu, W., Li, X., Tan, X., 2017. The new method on gas-water two phase steady-state productivity of fractured horizontal well in tight gas reservoir. Adv. Geo-Energy Res. 1 (2), 105–111. https://doi.org/10.26804/ager.2017.02.06.

Liu, H., Zhu, Z., Patrick, W., Liu, J., Lei, H., Zhang, L., 2020. Pore-scale numerical simulation of supercritical CO2 migration in porous and fractured media saturated with water. Adv. Geo-Energy Res. 4 (4), 419–434. https://doi.org/10.46690/ager.2020.04.07.

Masters, J.A., 1979. Deep basin gas trap, western Canada. AAPG Bull. 63 (2), 152–181. https://doi.org/10.1306/C1EA55CB-16C9-11D7-8645000102C1865D.

Pang, X., Jia, C., Wang, W., Chen, Z., Li, M., Jiang, F., Wang, Y., 2021. Buoyance-driven hydrocarbon accumulation depth and its implication for unconventional resource prediction. Geosci. Front. 12 (4), 101133. https://doi.org/10.1016/j.gsf.2020.11.019.

Qiao, J., Zeng, J., Jiang, S., Ma, Y., Feng, S., Xie, H., Hu, H., 2020. Role of pore structure in the percolation and storage capacities of deeply buried sandstone reservoirs: a case study of the Junggar Basin, China. Mar. Petrol. Geol. 113, 104129. https://doi.org/10.1016/j.marpetgeo.2019.104129.

Rushing, J.A., Newsham, K.E., Van Fraassen, K.C., 2003. October. Measurement of the two-phase gas slippage phenomenon and its effect on gas relative permeability in tight sandstone gas sands. SPE Annu. Tech. Conf. Exhib. https://doi.org/10.2118/84297-MS.

Sakhaee-Pour, A., Bryant, S.L., 2014. Effect of pore structure on the producibility of tight-gas sandstones. AAPG Bull. 98 (4), 663–694. https://doi.org/10.1306/08011312078.

Sneider, R.M., Tinker, C.N., Meckel, L.D., 1978. Deltaic environment reservoir types and their characteristics. J. Petrol. Technol. 30 (11), 1538–1546. https://doi.org/10.2118/6701-PA.

Wood, J.M., Sanei, H., 2016. Secondary migration and leakage of methane from a major tight-gas system. Nat. Commun. 7 (1), 1–9. https://doi.org/10.1038/ncomms13614.

Zhang, T., Javadpour, F., Li, X., Wu, K., Li, J., Yin, Y., 2020. Mesoscopic method to study water flow in nanochannels with different wettability. Phys. Rev. E 102 (1), 013306. https://doi.org/10.1103/PhysRevE.102.013306.

Zhao, K., Du, P., 2019. Performance of horizontal wells in composite tight gas reservoirs considering stress sensitivity. Adv. Geo-Energy Res. 3 (3), 287–303. https://doi.org/10.26804/ager.2019.03.07.

Zhao, W., Zhang, T., Jia, C., Li, X., Wu, K., He, M., 2020. Numerical simulation on natural gas migration and accumulation in sweet spots of tight reservoir. J. Nat. Gas Sci. Eng. 81, 103454. https://doi.org/10.1016/j.jngse.2020.103454.

Zhao, W., Jia, C., Jiang, L., Zhang, T., He, M., Zhang, F., Wu, K., 2021. Fluid charging and hydrocarbon accumulation in the sweet spot, Ordos Basin, China. J. Pet. Sci. Eng. 200, 108391. https://doi.org/10.1016/j.petrol.2021.108391.

Zhao, W., Jia, C., Song, Y., Li, X., Hou, L., Jiang, L., 2023. Dynamic mechanisms of tight gas accumulation and numerical simulation methods: narrowing the gap between theory and field application. Adv. Geo-Energy Res. 8 (3), 146–158. https://doi.org/10.46690/ager.2023.06.02.

Zhu, W., Liu, Y., Shi, Y., Zou, G., Zhang, Q., Kong, D., 2022. Effect of dynamic threshold pressure gradient on production performance in water-bearing tight sandstone gas reservoir. Adv. Geo-Energy Res. 6 (4). https://doi.org/10.46690/ager.2022.04.03.